Inorganic Chemistry

Article

pubs.acs.org/IC

$AuCd_4$: A Hume–Rothery Phase with VEC of 1.8 and Icosahedral and Trigonal-Prismatic Clusters as Building Blocks

Partha P. Jana*[,†] and Sven Lidin[†]

[†]CAS Chemical Centre, Lund University, Box 124, Getingevägen 60, Lund SE-22100, Sweden

Supporting Information

ABSTRACT: The η phase in the Au–Cd binary system has been synthesized, and the structure has been analyzed by single-crystal X-ray diffraction. The compound η-$AuCd_4$ crystallizes in the hexagonal space group $P6_3/m$ (No. 176). The unit cell contains ~273 atoms. The compound $AuCd_4$ represents a $\sqrt{3}a \times \sqrt{3}a \times c$ superstructure of the $AgMg_4$ type. The structure can be well described by icosahedral and trigonal-prismatic clusters. A phase transition to the high-temperature ε phase occurs exothermically at around 578 K. The compound is formed at a sharp valence electron concentration of 1.8 e/a. The compound can be understood within the framework of the Hume-Rothery stabilization mechanism.

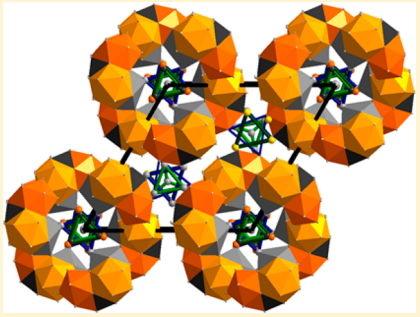

INTRODUCTION

Brass-like alloys occur at a certain ratio of the number of valence electrons to atoms (e/a), i.e., valence electron concentration (VEC). Such alloys are known as Hume-Rothery alloys or electron compounds.[1,2] In the Cu–Zn system, at different compositions, five different phases (i.e., α, β, γ, ε, and η) have been characterized. In many other systems of binary intermetallics, similar phases have been found. In the Cu–Zn system, the α and η phases are considered to be solid solutions of the parent elements, while the β and ε phases are stabilized at ratios of 21/14 and 21/12 e/a, respectively. The most complex structures are found for VEC values close to 21/13.[3−5] It is assumed that the γ-brass-type phase is stabilized at 21/13 e/a and a slight variation of VEC from 21/13 e/a results in structural modification of this phase: (i) electronic distortions or specific chemical ordering in the shells can be associated with a reduction of the rotational symmetry from cI to hR[6] or the translation symmetry from cI to cP,[7] (ii) $2 \times 2 \times 2$ superstructure of the γ-brass-type or related phase,[8−16] (iii) modulated structures of some Cd- and Zn-rich phases bearing a close resemblance to the respective cubic γ-brass-type phase,[17−21] and (iv) more complex and incommensurately modulated monoclinic δ''-$AuCd_{1.78}$ formed by an unquenchable phase transformation of γ-brass-type δ' phase.[22]

In 1936, Mott and Jones first interpreted the stabilization mechanism of electron compounds in terms of the interaction between the Fermi surface of radius k_F and the Brillouin zone characterized by a reciprocal lattice vector based on the nearly free electron (NFE) model. As a consequence, a pseudogap is formed by the lowering of the kinetic energy of the valence electrons across the Fermi level, and this plays a key role in stabilizing Hume-Rothery phases.[23,24] This pseudogap is also conspicuous in more detailed, state-of-the-art, electronic structure calculations.

In recent time, the Hume-Rothery rules have been extended for quasicrystals (QCs) and their crystalline approximants (QAs). The most relevant criterion for the formation of stable QCs is that the alloy should have a definite VEC. Band structure calculations on crystalline approximants confirmed that most of the QCs are stabilized by the Hume-Rothery mechanism. It is empirically determined that most stable QCs are formed if the e/a value is close to 1.7 (Bergman type) or 2.1 (Tsai type). Hence, VEC (e/a) can be considered to be the most convenient criterion to understand the stabilization of a large number of intermetallics including QCs and QAs.[25−29]

Recent investigations on the Cd-rich phase of the Au–Cd system (Figure 1) have uncovered new compounds in the ~20 atom % of Au that occur at a sharp VEC of 1.8 e/a. The phase was previously mentioned as $AuCd_5$, but the structure is not known to date. Moreover, the title compound $AuCd_4$ is of particular importance to a greater extent because it gives insight into the formation and stability of a new class of Hume-Rothery phases that are stabilized at 1.8 e/a. The class may include previously reported stoichiometric compounds: γ-$AgMg_4$[30] and λ-Al_4Mn.[31] The title compound can be described as a superstructure of $AgMg_4$. All of these previously mentioned intermetallic compounds in this class are situated in the region of QCs and QAs.

The present study is aimed at resolving the structure of the η phase[32] in the Au–Cd binary system.

EXPERIMENTAL SECTION

Syntheses. The η-$AuCd_4$ phase was synthesized by high-temperature reaction starting from the pure constituent elements Au

Special Issue: To Honor the Memory of Prof. John D. Corbett

Received: March 18, 2014
Published: June 17, 2014

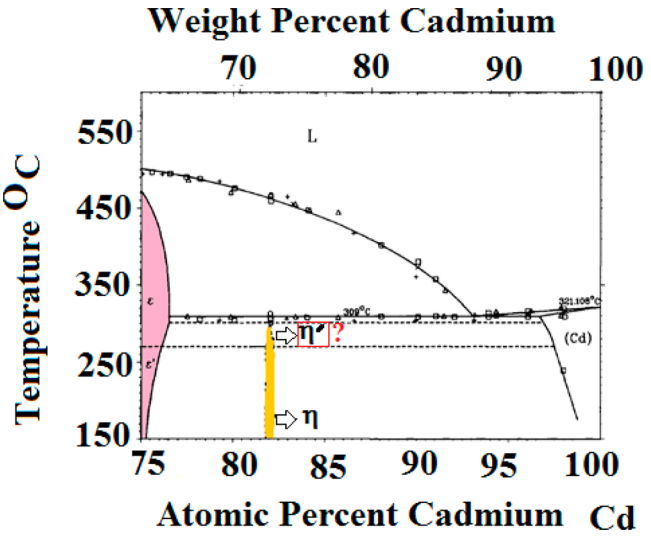

Figure 1. Phase diagram of the Cd-rich part of the Au−Cd system.[32]

(99.995%, Aldrich) and Cd (99.9999%, Chempur). Samples of precisely weighed metals (approximately 0.3 g each) were loaded and sealed in Ar-purged evacuated silica ampules (3 cm length and 0.8 cm diameter). The molar fraction x_{Au} of the mixtures was systematically varied between 0.14 and 0.25. The metals were heated at a rate of 194.4 K h^{-1} up to 773 K at which the ampules were kept for 200 h. The temperature was subsequently reduced to 473 K over a period of 240 h and annealed at this temperature for 200 h. Finally, the samples were either quenched in cold water or slowly cooled to ambient temperature. Products obtained from these reactions were silvery, brittle ingots, stable in air. Regardless of the composition, in each synthesis the phase produced was $AuCd_{\sim 4}$.

X-ray Diffraction Data Collection and Processing. In order to get reliable information about the composition of the Cd-rich phase, four distinct single crystals in the range $0.25 \leq x_{Au} \leq 0.16$ were studied by means of single-crystal X-ray diffraction. Suitable crystals were picked from the crushed sample and mounted onto a glass fiber, and diffraction intensities were measured with an Oxford Diffraction XCalibur Eos equipped with Mo Kα radiation (λ = 0.71073 Å, 50 kV, 40 mA) at room temperature of 293 K. Data collection and reduction were performed with the Oxford Diffraction Crysalis system. Structure solution and refinement were carried out using the *Jana2006* program.[33,34] Measurement details, atomic coordinates, site occupancy factors (SOFs), and equivalent isotropic displacement parameters are listed in Table 1. Further details are given in the Supporting Information (SI).

The powder diffraction data were collected by a STOE STADI MP diffractometer (Cu Kα_1 = 1.5406 Å, 40 kV, 40 mA, Mythen 1K detector). The diffractograms were recorded over the 2θ range 5−90° at room temperature.

Energy-Dispersive X-ray Analysis. The compositions of selected specimens were examined in a scanning electron microscope (a JEOL 3000 with a secondary electron detector), providing energy-dispersive X-ray spectrometry (EDS) spectra. EDS spectra were recorded from those samples that had been previously examined by single-crystal X-ray diffraction experiments.

Thermal Analysis. The thermochemical properties of the synthesized samples were studied in the temperature range 300−1373 K, employing a differential scanning calorimeter (Netzsch Instrument STA449 F3 Jupiter). Moreover, several differential thermal analysis (DTA) runs on a particular sample in the temperature range 250−400 °C were performed. Typically, 30−40 mg powder samples were placed in small alumina crucibles. An empty crucible of similar size was used as the reference. The experiments were carried out under a nitrogen atmosphere.

Electronic Structure Calculations. To understand the stability of these phases, ordered model compounds "$Au_{48}Cd_{224}$" and "$Ag_{16}Mg_{74}$" were constructed using the refined crystallographic results and used for calculation in the tight-binding, linear muffin-tin orbital (TB-LMTO) method with the atomic sphere approximation (ASA).[35−38] Exchange and correlation were treated in the von Barth−Hedin local density approximation.[39] All relativistic effects except spin−orbit coupling were taken into account by using a scalar relativistic approximation.[40] In ASA, space is filled with small, overlapping Wigner−Seitz (WS) spheres at each atomic site. The symmetry of the potential is considered to be spherical inside each WS sphere, and a combined correction takes the overlapping part into account. The radii of the WS spheres were optimized under the requirement that the overlapping potential should give the best possible approximation to the full potential by an automatic procedure.[41] A total of 18 empty spheres were needed to satisfy the LMTO volume criterion for "$Au_{48}Cd_{224}$". The basis set included Cd 5s and 5p orbitals and Au 6s, 6p, and 5d orbitals. For "$Ag_{16}Mg_{74}$", 23 empty spheres were needed and the basic sets were 5s, 5p, and 4d orbitals for Ag and 3s and 3p orbitals for Mg.

Table 1. Crystallographic Data for Single-Crystal Structure Refinement of $AuCd_{\sim 4}$

	C1	C2
chemical formula	$Au_{0.987}Cd_{4.07}$	$Au_{0.975}$ $Cd_{4.088}$
EDS formula	$Au_{1.0(2)}Cd_{4.1(2)}$	$Au_{1.0(1)}Cd_{4.1(2)}$
Pearson symbol	hP273	hP273
x_{Au}	0.195	0.193
cryst syst	hexagonal	hexagonal
space group; Z	$P6_3/m$ (No. 176); 54	$P6_3/m$ (No. 176); 54
a (Å)	21.326(1)	21.340(3)
c (Å)	14.125(1)	14.1212(17)
V ($\times 10^6$ Å^3)	5563.5(6)	5569.2(11)
ρ_{calcd} (Mg m^{-3})	10.504	10.4908
μ (mm^{-1})	55.43	55.039
cryst color	silvery with metallic luster	silvery with metallic luster
data collection diffractometer	four-circle diffractometer, Xcalibur, Eos	four-circle diffractometer, Xcalibur, Eos
radiation	Mo Kα	Mo Kα
monochromator	graphite	graphite
crystal-to-IP distance (mm)	50	50
T (K)	293(2)	293(2)
$2\theta_{max}$ (deg)	52.64	52.64
reflns measured	18155	20672
index range	$-25 \leq h \leq 29$	$-27 \leq h \leq 27$
	$-17 \leq k \leq 30$	$-23 \leq k \leq 26$
	$-19 \leq l \leq 16$	$-18 \leq l \leq 9$
completeness of the data set	0.9918	0.9955
abs corrn	multiscan	multiscan
no. of unique reflns	5544	4685
R_{int}	0.0644	0.0577
structure solution/ refinement	*JANA 2006* program package[33]	*JANA 2006* program package[33]
structure solution	*Superflip*[34]	*Superflip*[34]
no. of variables	243	243
no. of reflns used	5544	4685
obsd reflns [$I > 3\sigma(I)$]	3184	2800
R [$F^2 > 3\sigma(F^2)$]	0.0435	0.0379
$R(F)$ (all data)	0.0982	0.0651
k^a	0.0004	0.0004
wR(F^2) (all data)	0.0980	0.0829
GOF (all)	1.09	1.09
$\Delta\rho_{min}/\rho_{max}$ (e Å^{-3})	−3.95/4.21	−3.79/4.10

[a]Weighting scheme: $w = 1/[\sigma^2(I) + k(I)^2]$.

dx.doi.org/10.1021/ic500616t | *Inorg. Chem.* 2015, 54, 713−721

Table 2. Structural Data for $Au_{0.987}Cd_{4.07}$ (C1) and $Au_{0.975}Cd_{4.088}$ (C2)

atom	Wyckoff	site	SOF[a]	*x*/*a*	*y*/*b*	*z*/*c*
Au1	6h	m..		0.78242(5)	0.17358(5)	$^1/_4$
				0.78236(5)	0.17360(5)	$^1/_4$
Au2	6h	m..		0.50213(5)	−0.05466(5)	$^1/_4$
				0.50216(5)	−0.05464(5)	$^1/_4$
Au3	6h	m..		0.72265(5)	−0.11050(5)	$^1/_4$
				0.72269(5)	−0.11054(5)	$^1/_4$
Au4	12i	1		0.56967(3)	0.19071(3)	0.05117(5)
				0.56970(3)	0.19067(3)	0.05107(5)
Au5	12i	1		0.66819(4)	0.00416(4)	−0.08019(4)
				0.66824(4)	0.00419(4)	−0.08027(4)
Au6	6h	m..	0.633	0.71670(7)	0.23329(6)	$-^1/_4$
			0.629	0.71663(6)	0.23328(6)	$-^1/_4$
Cd6a	6h	m..	0.367	0.71670(7)	0.23329(6)	$-^1/_4$
			0.371	0.71663(6)	0.23328(6)	$-^1/_4$
Au7	12i	1	0.53	0.95624(15)	0.0970(5)	0.05108(18)
			0.47	0.95616(19)	0.0981(7)	0.0512(3)
Cd7′	12i	1	0.46	0.9650(8)	0.0760(12)	0.0517(4)
			0.55	0.9632(11)	0.0784(19)	0.0510(5)
Cd1	6h	m..		0.91495(10)	0.30552(9)	$^1/_4$
				0.91530(9)	0.30566(9)	$^1/_4$
Cd2	6h	m..	0.813	0.89012(12)	−0.14327(11)	$^1/_4$
			0.788	0.88953(11)	−0.14332(10)	$^1/_4$
Au2b	6h	m..	0.187	0.89012(12)	−0.14327(11)	$^1/_4$
			0.212	0.88953(11)	−0.14332(10)	$^1/_4$
Cd3	6h	m..		0.03564(10)	0.27458(12)	$^1/_4$
				0.03565(9)	0.27459(11)	$^1/_4$
Cd4	6h	m..		0.36332(10)	−0.07292(10)	$^1/_4$
				0.36334(9)	−0.07282(10)	$^1/_4$
Cd5	4f	3..		$^2/_3$	$^1/_3$	0.12643(18)
				$^2/_3$	$^1/_3$	0.12606(18)
Cd6	12i	1		0.49441(7)	0.05321(7)	0.13865(9)
				0.49419(7)	0.05304(7)	0.13838(9)
Cd7	12i	1		0.56042(8)	−0.04695(8)	0.06728(10)
				0.56059(8)	−0.04692(8)	0.06721(9)
Cd8	2c	−6..		$^2/_3$	$^1/_3$	$-^1/_4$
				$^2/_3$	$^1/_3$	$-^1/_4$
Cd9	12i	1		0.60483(8)	0.09099(7)	−0.03110(11)
				0.60477(7)	0.09099(7)	−0.03145(11)
Cd10	12i	1		0.73778(8)	0.10251(8)	0.07159(9)
				0.73776(7)	0.10249(7)	0.07164(9)
Cd11	6h	m..		0.59037(10)	−0.11571(11)	$^1/_4$
				0.59026(10)	−0.11569(10)	$^1/_4$
Cd12	12i	1		0.42545(7)	0.15838(7)	0.0547(1)
				0.42546(7)	0.15836(7)	0.0546(1)
Cd13	12i	1		0.70013(9)	−0.06491(8)	0.42923(10)
				0.70002(8)	−0.06495(8)	0.42909(9)
Cd14	12i	1		0.81434(7)	0.37995(8)	−0.14922(9)
				0.81437(7)	0.38015(7)	−0.14919(9)
Cd15	6h	m..		0.55162(11)	0.19674(10)	$^1/_4$
				0.55177(10)	0.19672(10)	$^1/_4$
Cd16	6h	m..		0.63732(11)	0.06076(12)	$^1/_4$
				0.63738(11)	0.06108(12)	$^1/_4$
Cd17	12i	1		0.69298(8)	0.21028(8)	0.1463(1)
				0.69307(8)	0.21036(8)	0.14624(9)
Cd18	12i	1		0.89935(7)	0.17390(7)	0.13393(10)
				0.89935(7)	0.17400(7)	0.13364(9)
Cd19	12i	1		0.77242(7)	0.16375(7)	−0.37071(9)
				0.77236(7)	0.16379(7)	−0.37069(9)
Cd20	12i	1		0.70640(7)	0.25540(7)	−0.05132(10)

dx.doi.org/10.1021/ic500616t | *Inorg. Chem.* 2015, 54, 713−721

Table 2. continued

atom	Wyckoff	site	SOF[a]	*x*/*a*	*y*/*b*	*z*/*c*
				0.70656(7)	0.25521(7)	−0.05143(9)
Cd21	12i	1		0.82594(8)	0.06523(8)	−0.04640(12)
				0.82581(7)	0.06530(8)	−0.04662(12)
Cd22	6h	m..		0.77268(15)	0.03775(12)	1/4
				0.77274(14)	0.03765(11)	1/4
Cd23	12i	1		0.96779(10)	0.11747(11)	−0.14657(11)
				0.96771(9)	0.11746(10)	−0.14659(11)
Cd24	4e	3..	0.522	1.00000	0	0.1316(4)
			0.51	1.00000	0	0.1320(4)
Cd24′	2a	−6..	0.543	1.00000	0	1/4
			0.548	1.00000	0	1/4

[a]Only fractional site occupancy factors (S.O.F.) are given.

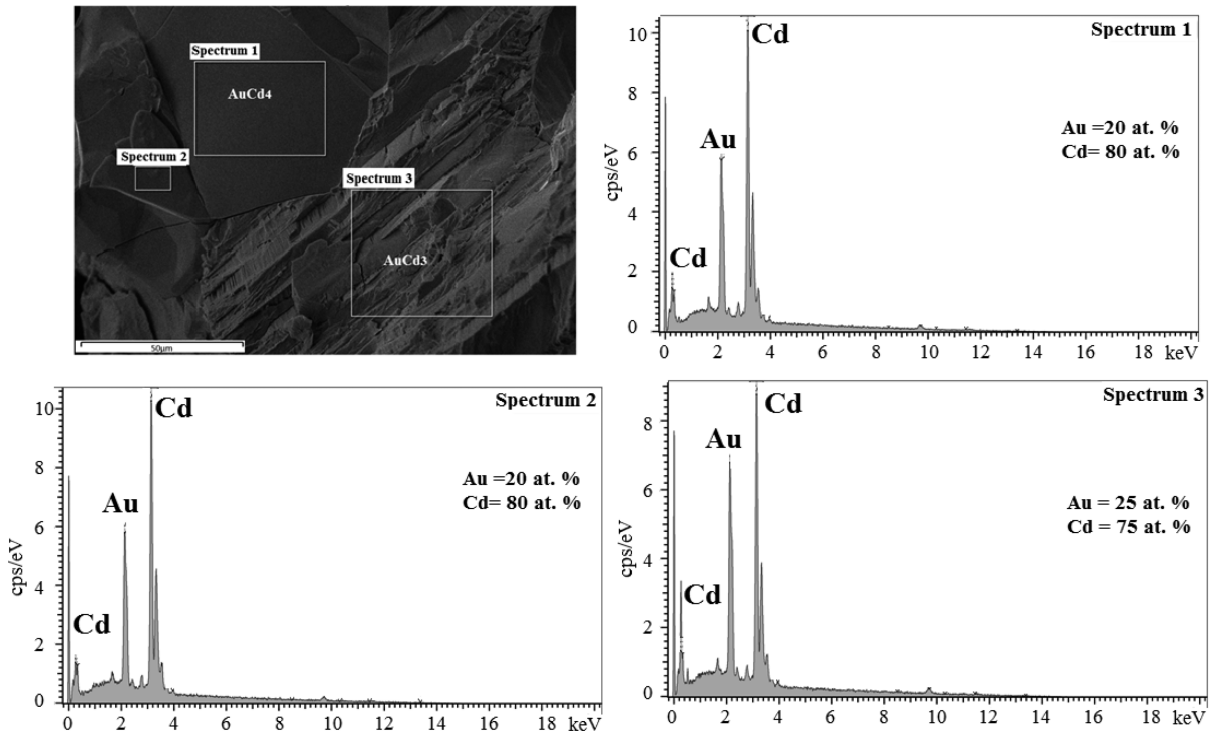

Figure 2. Scanning electron microscopy image (top left) and EDS spectra (top right, bottom) showing the coexistence of $AuCd_4$ with ε-$AuCd_3$. The spectra correspond to the rectangular surface indicated in the top left image.

The Brillouin zone integrations were accomplished on a 5 × 5 × 7 *k*-point mesh with the tetrahedron method.[42]

RESULTS

Structure Solution and Refinement. The structure was solved in the centrosymmetric space group $P6_3/m$ (No. 176) using *Superflip*.[34] Additional atomic positions were included from residual electron density maps after a preliminary cycle of refinement. At this stage, the structural refinement converged at $R(F) \approx 0.10$. Further improvement of the calculations was obtained by the chemical mixing of Au and Cd on those Au sites, which showed higher displacement parameters with respect to the normal in a first step, assuming those sites to be fully occupied (Cd2/Au2b and Au6/Cd6a). On the other hand, atomic sites showing noticeably large thermal displacement parameters were checked for occupancy and positional disorder. Atomic sites for which the refined occupancy factors deviated by less than the standard deviation from unity were reset to unity in the final refinement cycles. Local structural disorder phenomena were modeled by introducing split positions. There are several short distances in the structure (see Table 2), for instance, *d*(Cd24−Cd24′) and *d*(Au7−Cd7′). In no case does the sum of the SOFs of two such sites exceed unity, and the splits are explainable in terms of a set of locally ordered clusters. The independently refined SOFs of those adjacent atomic sites show the relationships SOF(Au7) + SOF(Cd7′) = 1 and SOF(Cd24) + SOF(Cd24′) = 1. (Note that, for clarity, Cd7′ and Cd24′ are referred to as Cd7a and Cd24a in the CIF file, respectively.) All disordered sites were refined with uncoupled occupation parameters except those that were assumed to be mixed occupied by both components. Harmonic atomic displacement parameters (ADP) were taken into account for all atoms. The final refinement including an isotopic extinction correction yields $R(F^2)$ $[F^2 > 3\sigma(F^2)]$ values between 0.03 and 0.040. Details concerning the atomic coordinates, equivalent isotropic displacement parameters, and anisotropic displacement parameters are listed in Table 2 and Supporting Information (S3 and S4), respectively.

dx.doi.org/10.1021/ic500616t | *Inorg. Chem.* 2015, 54, 713−721

Phase Analysis. The homogeneity range and constitution of the hexagonal η phase in the Au−Cd system were examined by means of preparative methods, X-ray diffraction, and EDS analyses. Chemical compositions analyzed by EDS are essentially in accordance with the composition outcome of the single-crystal X-ray structure refinement. The phase does not exhibit a discernible homogeneity range. The refined compositions from single-crystal X-ray diffraction experiments, and the results of EDS analyses for selected crystalline specimens can be found in Table 1. $AuCd_4$ coexists with $AuCd_3$ in the sample with nominal composition $x_{Au} = 0.22$ as observed by EDS analysis (Figure 2). The sample with nominal composition $x_{Au} = 0.14$ coexists with pure Cd droplets as the minority component.

Experimental and calculated powder X-ray diffraction patterns of η-$AuCd_4$ over the 2θ range 10−90° are shown in the SI (Figure S1).

Thermal analyses show that the η phase transforms to the ε phase at 578(1) K. The existence of the η' phase is uncertain. The phase transformation ($\eta \rightarrow \varepsilon$) is irreversible. A peak evolving at ca. 590 K showed up in DTA runs of differently composed samples. We may suggest that this feature is associated with a structural disorder upon heating in the ε phase, yet proof is still lacking. The ordered ε phase forms again at 578 K upon cooling (Figure S2 in the SI).

DISCUSSION

$AuCd_4$ forms a complex, partly disordered, $\sqrt{3}a \times \sqrt{3}b \times c$ superstructure of the γ-$AgMg_4$ phase. Binary $AuCd_4$ crystallizes in the space group $P6_3/m$ (No. 173) and contains 273 atoms in its unit cell. The structure contains 32 crystallographically independent sites: 5 Au, 22 Cd, 2 mixed Au/Cd (Au6/Cd6a and Cd2/Au2b), and 2 split sites (Au7/Cd7′ and Cd24/Cd24′). The structure of $AuCd_4$ may be described in terms of icosahedral and trigonal-prismatic clusters.

The structure can conveniently be divided into two motifs, with one being a mostly ordered network of icosahedra that form a cylindrical arrangement parallel to the c axis. Between (along $^1/_3$, $^2/_3$, z) and within (along 0, 0, z) the cylinders, a different arrangement of atoms create two different kinds of clusters based on trigonal-prismatic arrangements (Figure 3). The clusters between the cylinders display some occupational disorder, while the clusters within the cylinders display a combination of occupational and displacive disorder.

Five icosahedra form an icosahedral building unit. Among them, three Au-centered (Au1 and Au5) face-sharing icosahedra form a 31-atom unit built up by 41 tetrahedra. The addition of 2 more atoms (Cd2/Au2b and Au3) into the 31-atom unit generates a 33-atom icososahedral building unit (Figure 2). This unit comprises 50 tetrahedra. Clusters of this size partially interpenetrate. The 33-atom building unit can be extended along the [001] direction (Figure 3). The 33-atom building units are connected by the vertexes of Au-centered icosahedra and form a starlike zigzag tunnel. The tunnels are inhabited by trigonal-prismatic clusters as another building unit. The prismatic units are grouped about (0, 0, z), ($^1/_3$, $^2/_3$, z), and ($^2/_3$, $^1/_3$, z), as shown in Figure 3. Note that "clusters" are built up by the sets of symmetrically independent atoms, also called polyhedral shells. Here the cluster of trigonal prisms at (0, 0, z) referred to as Z consists of partially occupied Cd24′ (CC) and Cd24 (Cd_2 pair), a tricapped trigonal prism (TTP), and a positionally disordered outer trigonal-prismatic (OTP) shell. Positional disorder at the OTP site arises from physically meaningless short distances between Au7 and Cd7′, where Cd7′ forms a smaller OTP and Au7 forms a larger OTP (Figure 4 and Table 2).

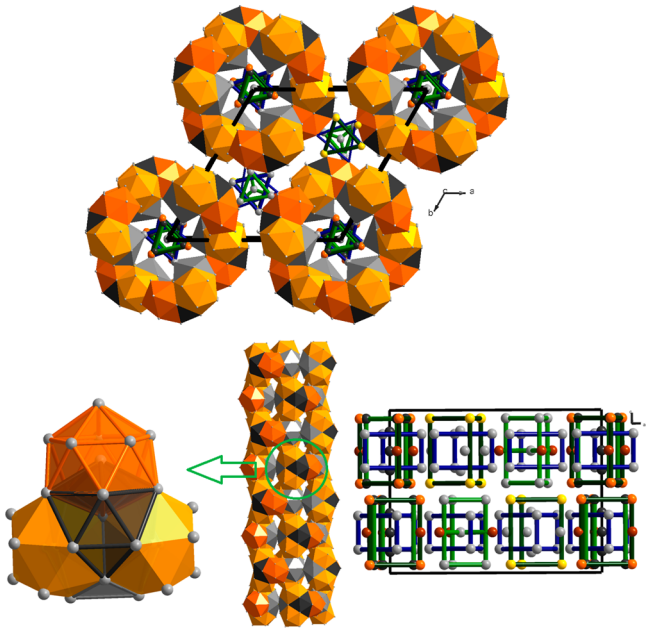

Figure 3. (Top) Representation of the structure of η-$AuCd_4$ along c: icosahedral and trigonal-prismatic clusters as building blocks. (Bottom left) 33-atom icosahedral building unit. (Bottom middle) Zigzag column of icosahedral building units along [001] connected by sharing the vertices of Au-centered icosahedra. (Bottom right) Arrangement units of trigonal-prismatic clusters in a unit cell. Au and Cd atomic sites with full occupancies are depicted in light gray and yellow, respectively. Mixed Au/Cd sites are in brown. Positionally disordered Au and Cd sites are represented in orange and deep gray, respectively.

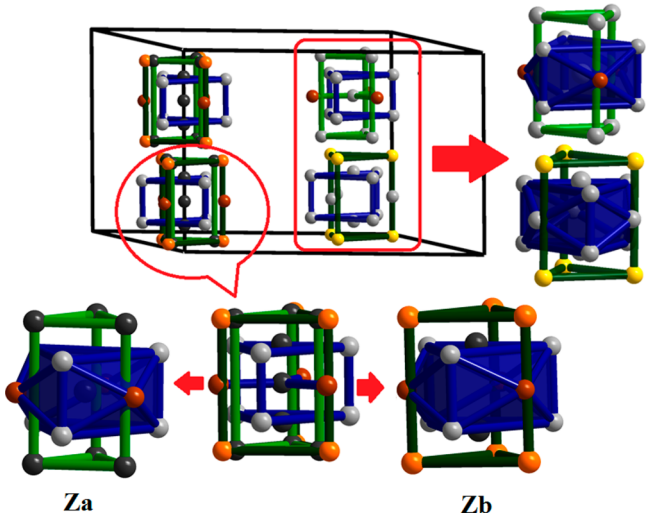

Figure 4. View of different arrangements of trigonal-prismatic clusters (denoted as Z). Clusters (Z) are grouped about (0, 0, z), ($^1/_3$, $^2/_3$, z), and ($^2/_3$, $^1/_3$, z), where $z = {}^1/_4$ and $^3/_4$. Cd-centered 16-atom cluster $Cd@Cd_6(Au/Cd)_3@Cd_6$ with the shell sequence CC, TTP, and OTP is referred as Z_a, whereas the 17-atom cluster $Cd_2@Cd_6(Au/Cd)_3@Au_6$ is represented as Z_b. Fully occupied Au and Cd atomic sites are depicted in light gray and yellow, respectively. Mixed Au/Cd sites are in brown. Split Au and Cd sites are represented in orange and deep gray, respectively.

dx.doi.org/10.1021/ic500616t | Inorg. Chem. 2015, 54, 713−721

The clear correlations between the independently refined occupation factors, SOF(Cd24) = 1 − SOF(Cd24′) and SOF(Au7) = 1 − SOF(Cd7′), can be rationalized by a simple exchange mechanism, where either a defect Cd-centered 16-atom cluster Z_a ($Cd@Cd_6(Au/Cd)_3@Cd_6$) with shell sequence CC, TTP, and OTP or a 17-atom cluster Z_b ($Cd_2@Cd_6(Au/Cd)_3@Au_6$) is situated around the high symmetry points (0, 0, $^1/_4$) and (0, 0, $^3/_4$) (Figure 3), respectively. The occupancies of Cd24 and Au7 are roughly equal, as are those of Cd24′ and Cd7′. Starting by identifying the building units of prismatic clusters about ($^1/_3$, $^2/_3$, z) and ($^2/_3$, $^1/_3$, z), we find that clusters Z_a and Z_b are present and are centered at the heights of Z of ($^1/_4$ and $^3/_4$) and ($^3/_4$ and $^1/_4$), respectively.

There is a close structural resemblance of $AuCd_4$ to γ-$AgMg_4$ (Figure 5) and λ-Al_4Mn (Figures 6 and 7). All compounds

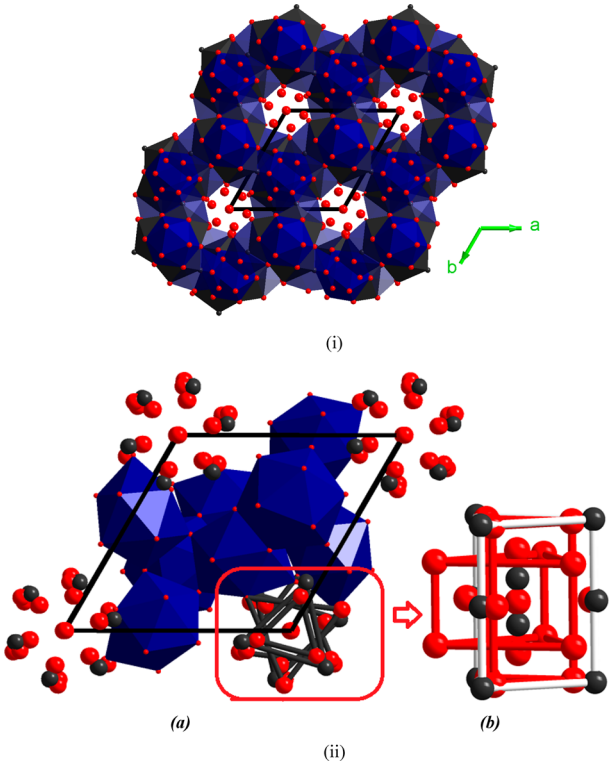

Figure 5. (i) Unit cell of the γ-$AgMg_4$: icosahedral building units. Ag- and Mg-centered icosahedra are depicted by blue and dark gray, respectively. Ag and Mg sites are depicted in dark gray and red, respectively. (ii) (a) Structure of γ-$AgMg_4$ icosahedra (blue) and trigonal-prismatic clusters as basic building units. View of disordered trigonal-prismatic clusters along [001] indicated in the red box, (b) Side view of the trigonal-prismatic cluster as the basic building unit. Ag and Mg sites are depicted in dark gray and red, respectively.

crystallize in the hexagonal space group $P6_3/m$. The cell parameters of γ-$AgMg_4$ are a =12.4852(8) Å and c = 14.4117(9) Å. Like $AuCd_4$, the crystal structure of this intermetallic compound contains building blocks of icosahedra and trigonal-prismatic cluster as the fundamental structural units. Distinct structural disorder is confined in the prismatic clusters (Figure 5).

The crystal structure of the λ-Al_4Mn phase crystallizes in $P6_3/m$ with a = 28.382(9) Å and c = 12.389(2) Å. All of the Mn sites have icosahedral coordination except two. Those two Mn sites have TTP coordination (Figures 6 and 7). Like $AuMg_4$ and $AuCd_4$, the structure has two basic building units:

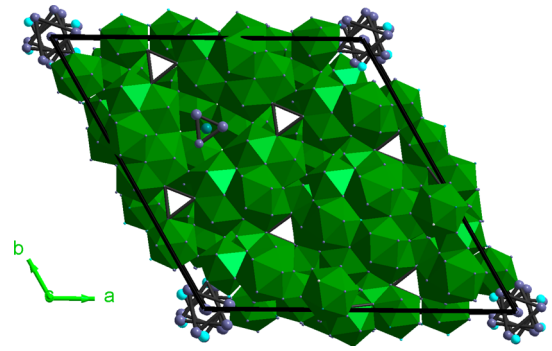

Figure 6. Structure of γ-Al_4Mn building blocks of icosahedra and trigonal-prismatic clusters.

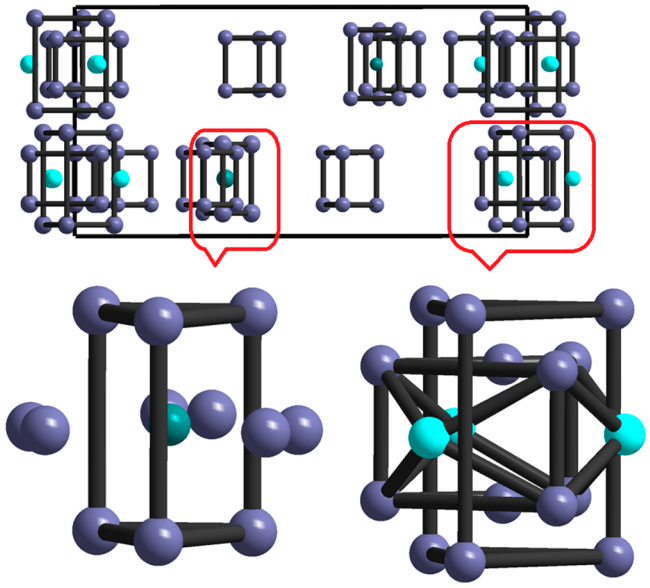

Figure 7. Presentation of different arrangements of trigonal-prismatic clusters in the structure of Al_4Mn. Atomic sites of Al, Mn, and mixed (Al/Mn) are depicted by blue-gray, teal, and turquoise, respectively.

icosahedra and trigonal prisms. Disorder phenomena in Al_4Mn are mainly part of the trigonal-prismatic clusters.

An extended structure is a Hume-Rothery structure if its electronic structure depends primarily on s- and p-orbital interactions. This means that d orbitals of the constituent atomic sites are filled and, for the most part, are not involved in bonding.

A straightforward approach is simply to fill the d orbitals completely. The valence d shells of Au, Ag, and Cd are already full: $5d^{10}5s^1$, $4d^{10}5s^1$, and $4d^{10}5s^2$, respectively. Hence, Au and Ag contribute 1 electron each, Cd contributes 2, and Al contributes 3. Mn has a half-filled d shell, $3d^54s^2$. Therefore, in order to fill its d shell, Mn contributes −3 electrons, although the valence-electron contribution by 3d metals like Mn remains ambiguous. In $AuCd_4$, $AgMg_4$, and Al_4Mn, this counting scheme gives VEC = 1.8. e/a. For electron compounds, it is assumed that disorder phenomena on various crystallographic sites are crucial to keep VEC nearly constant.

It is well-known that the valence of a transition element depends on alloying components. In the present case of the Al_4Mn alloys, it is difficult to evaluate VEC (e/a) because of the presence of the transition element Mn. The valence-electron contribution by 3d metals like Mn always remains controversial.

dx.doi.org/10.1021/ic500616t | Inorg. Chem. 2015, 54, 713−721

According to the first hypothesis (according to Hume-Rothery), valence electrons for transition elements with nonfilled d shells were assumed to be zero. The valence of Mn proposed by Raynor (1949) is −3.66 for Al-rich intermediate phases, which explains beautifully the formation of Al−Mn QCs. The valence of Mn proposed by Haworth and Hume-Rothery (1952) for the calculation of e/a is 1.9, which explains the formation of the α/β-brass-type Cu−Zn(Al)−Mn alloys. The electrons per atom ratio e/a for Mn, when dissolved in polyvalent metals like Al and Zn, is derived as 1.05 from the NFE approximation. Moreover, in the calculation based on s, p, and d electrons, the valance considered for Mn is 7.[28]

Electronic Structure. It is convenient to use the ordered model compound $Au_{48}Cd_{224}$ (hP272) to perform electronic structure calculations to understand the stability of the η phase in the Au−Cd binary system (see Table S1 in the SI). The model compound is a close approximation to the observed composition. The density of state (DOS) and crystal orbital Hamilton populations (COHP) curves of "$Au_{48}Cd_{224}$" are presented in Figures 8 and 9. The overall shape of the total

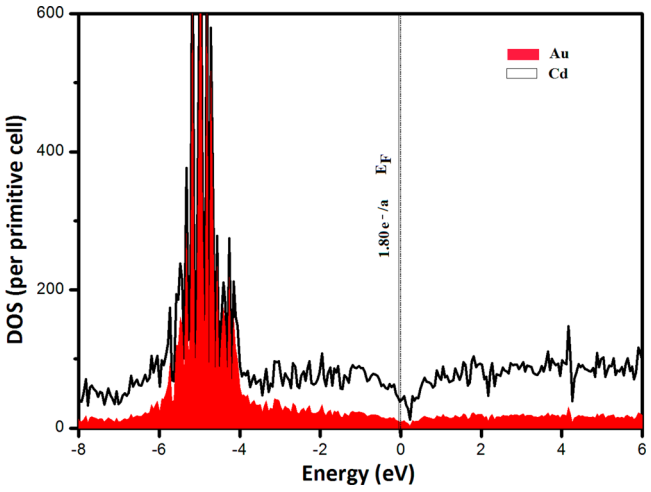

Figure 8. Representation of the total DOS curves of the model compound $Au_{48}Cd_{224}$. The Fermi level (E_F) for the model compound is depicted by the dotted line. Assuming a rigid band approximation, the Fermi level of the real composition $AuCd_4$ (VEC = 1.80 e/a) is marked by the solid line.

DOS curve is a parabola, which is a feature of the free-electron DOS, superimposed with the large peak of Au 5d bands at ca. −4 to −6 eV as well as a wide, flat state-deficient region, i.e., a pseudogap, at ca. −0.5 to 0.5 eV. Au 5d bands that are mainly concentrated within such a narrow energy range, significantly below E_F, discern their localized, semicore-state character. The Fermi level for "$Au_{48}Cd_{224}$" (VEC = 1.82 e/a, marked by the dotted line) falls into this pseudogap on the DOS curve. Assuming a rigid band approximation, the Fermi level of the observed composition (VEC = 1.80 e/a, marked by the solid line) is also located in the pseudogap. All of these characteristics in the DOS can also be found in brass-like phases, QCs/QAs, or Hume-Rothery phases, which indicates that η-$AuCd_4$ is stabilized through the same electronic mechanism: the interaction between the Fermi surface and the Brillouin-Jones zone boundary.

There is no short Au−Au interaction present in this structure. This indicates that the structure of η-$AuCd_4$ is stabilized by Au−Cd and Cd−Cd interactions. In the COHP

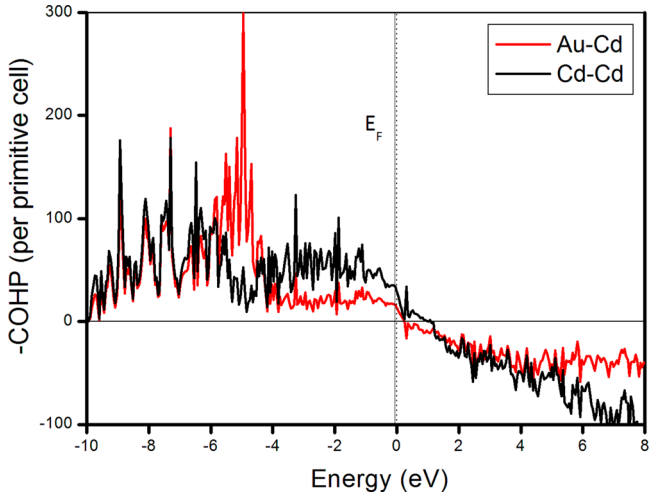

Figure 9. COHP curves of $Au_{48}Cd_{224}$. The Fermi levels (E_F) for the experimentally observed composition are depicted by the solid black line, assuming a rigid band approximation.

curve, E_F is located slightly below (Au−Cd and Cd−Cd) the bonding−antibonding crossovers. The states are strongly bonding below the pseudogap and strongly antibonding above it.

To test the stabilization mechanism of this group of compounds, we studied the electronic structure of the compound Ag_9Mg_{37} (hP92; e/a = 1.8). An ordered model structure, Ag_8Mg_{37} (hP90), was built by using the experimental structure of Ag_9Mg_{37}. Details regarding the model structure are given in the SI Table S2. Figure 10 shows the electronic DOS

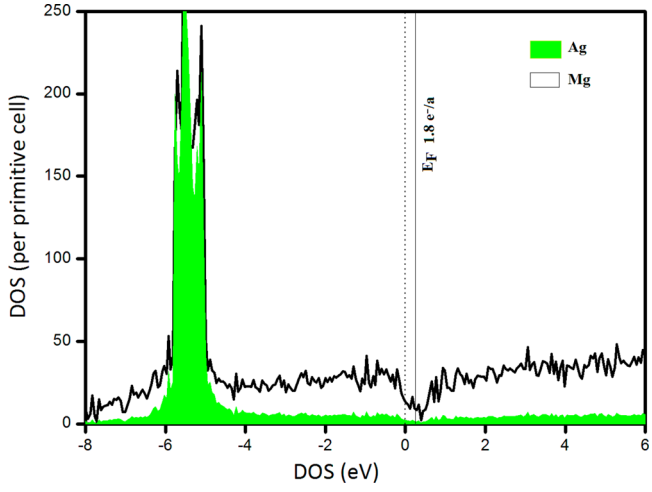

Figure 10. Representation of the total DOS curves of the model compound Ag_8Mg_{37}. The Fermi levels (E_F) for the model compound is depicted by the dotted line. Assuming a rigid band approximation, the Fermi level of the reported composition Ag_9Mg_{37} (VEC = 1.80 e/a) is marked by the solid line.

curve calculated for "Ag_8Mg_{37}", which is a close approximation to the reported composition. In the total DOS curve, the Ag 4d band is (ca. −4 to −6 eV) below the calculated Fermi level. There is also a distinct pseudogap, which ranges from around ca. −0.2 to 0.7 eV, and the Fermi level for the reported compound Ag_9Mg_{37} (VEC = 1.8 e/a) is located at the pseudogap (Figure 10), which is a feature that can be observed

dx.doi.org/10.1021/ic500616t | Inorg. Chem. 2015, 54, 713−721

in η-$AuCd_4$ phases and indicates that this compound is also stabilized by the Hume-Rothery mechanism.

It should be noted that the Fermi level for the real composition does not fall at the minima of the pseudogap, but it remains inside the range shown in Figure 8. This is a very common feature for many brass-type/related compounds, CMAs, and QCs.

For both compounds, the ideal VEC is actually higher than 1.8. The minimum of the pseudogap occurs somewhere at ca. 0.2 eV, but in a binary compound with a significant difference in metallic radii (numbers), the geometrical factor must also be considered. The ideal VEC values are also expected to be different for compounds with different ratios between capped trigonal prisms and icosahedra, but these differences should be small.

Common Features. The structures of the three phases η-$AuCd_4$, γ-$AgMg_4$, and λ-Al_4Mn have many common features, in spite of the variations in the complexity of the structures. Common features are as follows: (i) They all form line compounds without a perceptible homogeneity range, although they contain substitutional and positional disorder. The composition is MX_4 for all of the compounds. (ii) The compounds are formed at a sharp VEC of 1.8 e/a. The stability of the compounds can be understood by the Hume-Rothery stabilization mechanism. (iii) The structure of the three compounds can be described by icosahedra and trigonal-prismatic clusters as basic building units. Cluster types of the disordered part for all three compounds show resemblances in appearances and are mainly confined to trigonal-prismatic clusters.

Relationship to Some Hexagonal Approximants of QCs. Some closely related hexagonal phases with the same or nearly the same c values (varying between 12.4 and 14.4 Å) but with various a parameters (12.4, 21.3, 28.4, and 40.7 Å) are listed in Table 3. In Table 4, a summary of their relationships among their lattice parameters a is given by rescaling to parameter c = 14.1 Å for the mentioned compounds to make them readily comparable.

Table 3. Some Closely Related Hexagonal Phases

phase	space group	a (Å)	c (Å)	literature
γ-$AgMg_4$	$P6_3/m$	12.4852	14.4117	Kudla et al.[30]
η-$AuCd_4$	$P6_3/m$	21.326	14.125	present work
λ-Al_4Mn	$P6_3/m$	28.382	12.389	Franzen and Kreiner[31]
$Al_{80.61}Cr_{10.71}Fe_{8.68}$	$P6_3/m$	40.0	12.4	Sui et al.[43]
		40.687	12.546	Mo et al.[43−45]

CONCLUSION

The syntheses and structures of the η region in the Au−Cd system reveals the existence of a $\sqrt{3}a \times \sqrt{3}b \times c$ superstructure of the γ-$AgMg_4$-type phase, $AuCd_4$, without a discernible homogeneity range. The structure can be described using icosahedra and trigonal-prismatic clusters as basic building units. Various kinds of disorder on the trigonal-prismatic clusters retain VEC at a value of 1.8 e/a, which is assumed to confer the stability to a new class of Hume-Rothery phases. Electronic structure calculations show that the compound is metallic in nature with the presence of pseudogaps at the Fermi levels, which explains the formation of the electron compound within the framework of the Hume-Rothery stabilization mechanism.

Table 4. Relationship to the Related Hexagonal Phases

phase	a (Å)	c (Å)[a]	relationship
γ-$AgMg_4$	12.24	14.1	12.24
η-$AuCd_4$	21.3	14.1	$12.24 \times \sqrt{3} = 21.2$
λ-Al_4Mn	32.3	14.1	$12.24 \times \sqrt{7} = 32.4$
$Al_{80.61}Cr_{10.71}Fe_{8.68}$	45.7	14.1	$12.24 \times \sqrt{14} = 45.7$

[a]Rescale to c = 14.1 Å for all of the above-mentioned structures.

ASSOCIATED CONTENT

Supporting Information

Atomic displacement parameters, model structures Au_8Mg_{37} and $Au_{48}Cd_{224}$, a Rietveld profile fit, thermochemical analysis, and X-ray crystallographic files in CIF format. This material is available free of charge via the Internet at http://pubs.acs.org.

AUTHOR INFORMATION

Corresponding Author

*E-mail: Partha.Jana@chem.lu.se.

Notes

The authors declare no competing financial interest.

ACKNOWLEDGMENTS

The authors thank VR - the Swedish National Science Research Council, for financial support.

REFERENCES

(1) Hume-Rothery, W. *J. Inst. Met.* **1926**, *35*, 309.
(2) Hume-Rothery, W.; Raynor, G. V. *The Structure of Metals and Alloys*; Institute of Metals: London, U.K., 1954.
(3) Brandon, J. K.; Brizard, R. Y.; Chieh, P. C.; McMillan, R. K.; Pearson, W. B. *Acta Crystallogr., Sect. B* **1974**, *30*, 1412−1417.
(4) van Heidenstam, O.; Johansson, A.; Westman, S. *Acta Chem. Scand.* **1968**, *22*, 653−661.
(5) Gourdon, O.; Gout, D.; Williams, D. J.; Proffen, T.; Hobbs, S.; Miller, G. J. *Inorg. Chem.* **2007**, *46*, 251−260.
(6) Brandon, J. K.; Pearson, W. B.; Riley, P. W.; Chieh, C.; Stokhuyzen, R. *Acta Crystallogr., Sect. B* **1977**, *33*, 1088−1095.
(7) Kisi, E. H.; Brown, J. D. *Acta Crystallogr., Sect B* **1991**, *47*, 835−843.
(8) Mahne, S.; Harbrecht, B. *J. Alloys Compd.* **1994**, *203*, 271−279.
(9) Jana, P. P.; Lidin, S. *CrystEngComm* **2013**, *15*, 745−753.
(10) Koster, A. S.; Schoone, J. C. *Acta Crystallogr., Sect. B* **1981**, *37*, 1905−1907.
(11) Nasch, T.; Jeitschko, W. *J. Solid State Chem.* **1999**, *143*, 95−103.
(12) Thimmaiah, S.; Richter, K. W.; Lee, S.; Harbrecht, B. *Solid State Sci.* **2003**, *5*, 1309−1317.
(13) Hornfeck, W.; Thimmaiah, S.; Lee, S.; Harbrecht, B. *Chem.—Eur. J.* **2004**, *10*, 4616−4626.
(14) Jana, P. P. *J. Alloys Compd.* **2014**, *610*, 55−61.
(15) Jana, P. P.; Henderson, R.; Harbrecht, B.; Lidin, S. *Inorg. Chem.* **2013**, *52*, 4812−4818.
(16) Jana, P. P.; Pankova, A.; Lidin, S. *Inorg. Chem.* **2013**, *52*, 11110−11117.
(17) Schmidt, J.; Lee, S.; Fredrickson, D. C.; Conrad, M.; Sun, J.; Harbrecht, B. *Chem.—Eur. J.* **2007**, *13*, 1394−1410.
(18) Gourdon, O.; Miller, G. J. *Chem. Mater.* **2006**, *18*, 1848−1856.
(19) Gourdon, O.; Izaola, Z.; Elcoro, L.; Petricek, V.; Miller, G. J. *Philos. Mag.* **2006**, *86*, 419−425.
(20) Jana, P. P.; Lidin, S. *Inorg. Chem.* **2012**, *51*, 9893−9901.
(21) Jana, P. P.; Lidin, S. *Eur. J. Inorg. Chem.* **2013**, *2013* (1), 91−98.
(22) Jana, P. P.; Lidin, S. *Inorg. Chem.* **2013**, *52*, 12980−12985.

(23) Pearson, W. B. *The Crystal Chemistry and Physics of Metals and Alloys*; Wiley-Interscience: New York, 1972; pp 80−133.
(24) Pettifor, D. G. *Bonding and Structure of Molecules and Solids*; Oxford Science Publications: Oxford, U.K., 1995.
(25) Tsai, A.-P. *Chem. Soc. Rev.* **2013**, *42*, 5352−5365.
(26) Tsai, A.-P. *Acc. Chem. Res.* **2003**, *36*, 31−38.
(27) Tsai, A.-P. *J. Non-Cryst. Solids* **2004**, *334&335*, 317−322.
(28) Mizutani, U. *Hume-Rothery Rules for Structurally Complex Alloy Phases*; Taylor & Francis group: New York, 2010.
(29) Ishii, Y.; Fujiwara, T. *J. Non-Cryst. Solids* **2004**, *334&335*, 336−341.
(30) Kudla, C.; Prots, Y.; Leineweber, A.; Kreiner, G. *Z. Kristallogr.* **2005**, *220*, 102−114.
(31) Kreiner, G.; Franzen, H. *J. Alloys Compd.* **1997**, *261*, 83−104.
(32) Okamoto, H.; Massalski, T. B. *Bull. Alloy Phase Diagrams* **1986**, *7*, 52−67.
(33) Petricek, V.; Dusek, M.; Palatinus, L. *Jana 2006: The Crystallographic Computing System*; Institute of Physics: Praha, Czech Republic, 2006.
(34) Palatinus, L.; Chapuis, G. *J. Appl. Crystallogr.* **2007**, *40*, 786−790.
(35) Andersen, O. K. *Phys. Rev. B* **1975**, *12*, 3060−3083.
(36) Andersen, O. K.; Jepsen, O. *Phys. Rev. Lett.* **1984**, *53*, 2571−2574.
(37) Andersen, O. K.; Jepsen, O.; Glötzel, D.; Lambrecht, W. R. L. *Highlights of Condensed Matter Theory*; North-Holland: New York, 1985.
(38) Andersen, O. K. *Phys. Rev. B* **1986**, *34*, 2439−2449.
(39) von Barth, U.; Hedin, L. *J. Phys. C* **1972**, *5*, 1629−1642.
(40) Koelling, D.; Harmon, B. N. *J. Phys. C* **1977**, *10*, 3107−3114.
(41) Jepsen, O.; Andersen, O. K. *Z. Phys. B* **1995**, *97*, 35−47.
(42) Blçchl, P. E.; Jepsen, O.; Andersen, O. K. *Phys. Rev. B* **1994**, *49*, 16223−16233.
(43) Sui, H. X.; Li, X. Z.; Kuo, K. H. *Philos. Mag. Lett.* **1999**, *79*, 181−185.
(44) Mo, Z. M.; Zhou, H. Y.; Kuo, K. H. *Acta Crystallogr., Sect B* **2000**, *56*, 392−401.
(45) Zou, X. D.; Mo, Z. M.; Hovmöller, S.; Li, X. Z.; Kuo, K. H. *Acta Crystallogr., Sect. A* **2003**, *59*, 526−539.